CHEMISTRY OF MATERIALS

Communication

pubs.acs.org/cm

Cross Relaxation Induced Pure Red Upconversion in Activator- and Sensitizer-Rich Lanthanide Nanoparticles

Wei Wei,[†] Yan Zhang,[†] Rui Chen,[‡] Julian Goggi,[§] Na Ren,[⊥] Ling Huang,[⊥] Kishore K. Bhakoo,[§] Handong Sun,[‡,∥] and Timothy Thatt Yang Tan*[,†]

[†]School of Chemical and Biomedical Engineering, Nanyang Technological University, 62 Nanyang Drive, Singapore 637459, Singapore

[‡]Division of Physics and Applied Physics, School of Physical and Mathematical Sciences, Nanyang Technological University, 21 Nanyang Link, Singapore 637371, Singapore

[∥]Centre for Disruptive Photonic Technologies (CDPT), Nanyang Technological University, Singapore 637371, Singapore

[§]Singapore Bioimaging Consortium (A*STAR), Helios, 07-10, 11 Biopolis Way, Singapore 138667, Singapore

[⊥]Institute of Advanced Materials, Nanjing University of Technology, Nanjing 210009, China

Supporting Information

Lanthanide-doped upconversion nanoparticles (UCNPs) have been widely applied in a variety of areas such as optical devices, sensing, and therapeutics.[1] Their advantages include near-infrared (NIR) excitation, low cytotoxicity, weak autofluorescence, high chemical stability, and low photobleaching, which make them more desirable than conventional organic dyes or quantum dots for bioimaging application.[2] In particular, the UCNPs, which have both emission and excitation wavelengths located within the "tissue optical window" (spanning approximately from 650 to 1200 nm), are more suitable for deep tissue imaging.[3] However, the commonly investigated lanthanide activators such as Tm^{3+} and Er^{3+} ions contain abundant metastable excited states, and the dominant emission usually lies in the nonred region with relatively low red emission intensity.[4] Hence, a strategy to boost the red emission intensity will be useful for UC applications, especially for deep tissue imaging.

Cross relaxation (CR) among the activators is often perceived as deleterious,[5] and thus its ability to regulate the UC red emission output is often overlooked. To the best of our knowledge, the concentration of the activator in UCNPs is usually constrained below 2 mol % to eliminate the energy loss caused by CR.[6] A systematic investigation on UC behavior with heavy activator doping is almost nonexistent. In this work, we report, for the first time, evidence of approaching 100% red emission output in the visible region through CR effect relying solely on activator interaction (Figure 1a,b). This strategy based on CR effect is not only successful in achieving pure red 696 or 660 nm UC emission but could also act as an alternative approach for precise UC color tuning and provide further insight into the UC mechanism. Among all the hosts, the selection of sensitizer-rich $NaYbF_4$ can vastly improve 696 nm red emission intensity for Tm^{3+} doped UCNPs compared with low sensitizer (20% Yb^{3+}) and activator (1% Tm^{3+}) UCNPs. We have also shown that the same strategy can be used to enhance the 660 nm red emission intensity for Er^{3+} doped UCNPs. This is attributed to the boost in red emission yield in the visible region, resulted from a collaborative effect of CR and the increase in sensitizer content. In addition, the surface-modified $NaYbF_4$ UCNPs are shown to be superior compared to a clinical iodinated CT contrast agent (Iohexol) due to the high X-ray absorption coefficient of Yb^{3+} ions (e.g., Yb: 6.91 cm^2/g, I: 3.51 cm^2/g at 80 keV; Yb: 3.88 cm^2/g, I: 1.94 cm^2/g at 100 keV).[7] Therefore, the activator- and sensitizer- rich UCNPs can serve as a potential multifunctional material for CT/fluorescence dual-modal deep tissue imaging.

In order to minimize CR energy loss, sensitizer-rich $NaYbF_4$ host was selected and prepared by a well-established coprecipitation method in high-boiling-point solvents.[8] Transmission electron microscopy (TEM) shows the size and morphology of our as-prepared UCNPs (Figure 1c) with an average diagonal length of 100 nm (Supporting Information Figure S1). The X-ray diffraction (XRD) pattern (Figure 1d) confirms their hexagonal-phase structure (JCPDS No. 27-1427). In general, efficient lanthanide UC is mainly restricted to Tm^{3+}, Er^{3+}, and Ho^{3+} ions as activators.[9] The UC emission spectra of the above activators doped in $NaYbF_4$ UCNPs with their content varying from low to high were determined. With the increase in activator concentration, it was observed that the predominant emission for Tm^{3+} doped UCNPs shifts from 475 to 696 nm, while for Er^{3+} doped $NaYbF_4$ UCNPs, it shifts from 540 to 660 nm (Figure 1b). The photographs in Figure 1a depict visual evidence of the red emission dominant process. However, for Ho^{3+} doped $NaYbF_4$ UCNPs, we only observed an attenuation of emission intensity without any dominant emission shift (Supporting Information Figure S2). We deduce that the dominance in red emission and the quenching in nonred emission are attributed to the increased CR effect among the activators as their concentration increases.[10] Considering the effect of varying Yb^{3+} sensitizer concentration on UC color tuning based on a previous study,[11] we further studied the UC spectra of $NaYF_4$, $NaGdF_4$, and $NaLuF_4$ microrods with Yb^{3+} sensitizer fixed at 20 mol %. The results (UC spectra in Supporting Information Tables S1, S2, and S3) are consistent with that of $NaYbF_4$. Consequently, we conclude that the red emission dominant and nonred emission

Received: June 21, 2014
Revised: August 17, 2014
Published: August 21, 2014

dx.doi.org/10.1021/cm5022382 | Chem. Mater. 2014, 26, 5183−5186

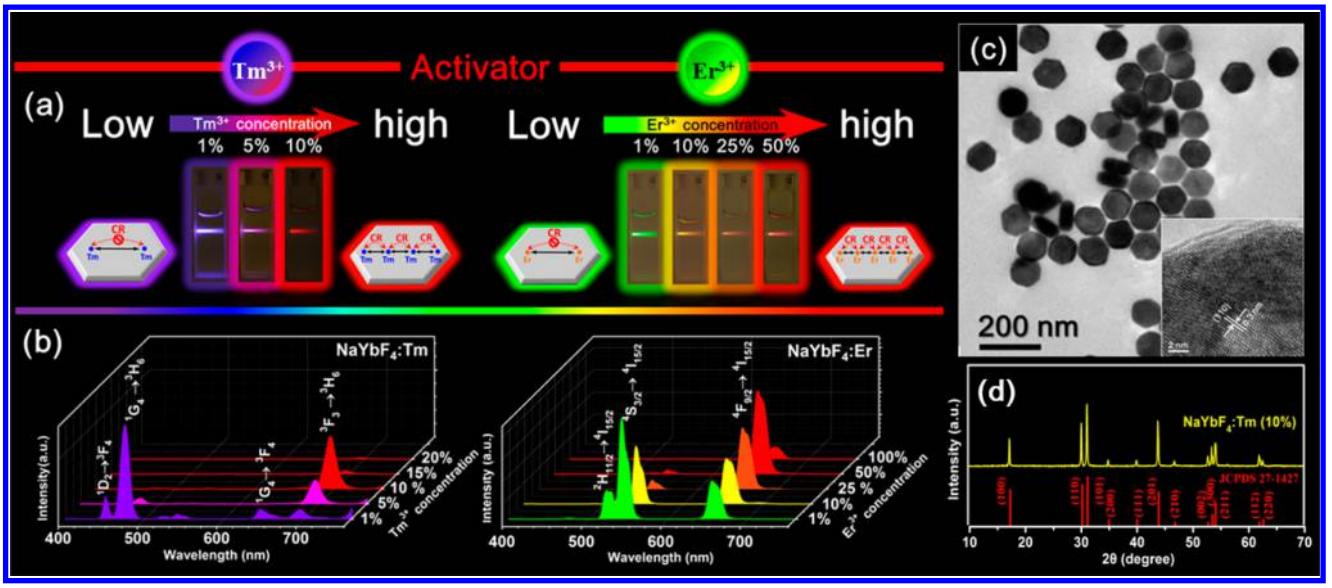

Figure 1. (a) Schematic illustrations of CR effect induced pure red UC emission with the increasing of activator (Tm^{3+}, Er^{3+}) concentration and the corresponding fluorescence photographs of $NaYbF_4$:Tm and $NaYbF_4$:Er UCNPs with the concentration of the activator varying from low to high. (b) UC emission spectra of 1, 5, 10, 15, and 20 mol % Tm^{3+} ions doped $NaYbF_4$:Tm and 1, 10, 25, 50, and 100 mol % Er^{3+} ions doped $NaYbF_4$:Er UCNPs. The spectra were recorded with 1 wt % UCNPs dispersed in hexane under 980 nm laser excitation at a power of 600 mW. Note: The typical UC emission spectra of $NaYbF_4$:Tm UCNPs from 300 to 900 nm (covering UV and NIR region) can be found in Supporting Information Figure S11. (c) A typical TEM image of the as-synthesized $NaYbF_4$:Tm (10%) UCNPs. Inset shows the corresponding HRTEM image. (d) XRD pattern of the $NaYbF_4$:Tm (10%) UCNPs.

quenching phenomenon is caused by a single factor, namely, the CR effect among the activators at high content.

To demonstrate that heavy activator doping can realize extremely high yield of red emission in the visible region, we determined the percentage of red emission output in 20 mol % Yb^{3+} doped $NaYF_4$, $NaGdF_4$, and $NaLuF_4$ microrods with different activator contents. By analyzing the UC spectra in Supporting Information Tables S1, S2, and S3, almost 100% red emission output can be generated from the 10 mol % Tm^{3+} (Figure 2a) and 50% Er^{3+} (Figure 2b) doped microrods using different host materials. Therefore, Figure 2a,b clearly shows that CR can serve as a tool for manipulating UC color output.

Furthermore, we found that significantly more intense pure red 696 and 660 nm emissions can be produced from sensitizer-rich $NaYbF_4$ host. Although the 696 nm signal could be detected from 20% Yb^{3+}/10% Tm^{3+} doped $NaYF_4$ UCNPs or $NaGdF_4$, $NaLuF_4$, and $NaYF_4$ microrods, it could not be visually observed. The clearly visible 696 nm emission from $NaYbF_4$:Tm (10%) (Figure 1) suggests that the increasing of sensitizer Yb^{3+} plays a crucial role in intensifying UC emission intensity at high activator content. To demonstrate that an appropriate increment of both sensitizer and activator is capable of enhancing red emission, we evaluated and compared the integral of the various red emission intensities and found that the intensity for 696 nm from $NaYbF_4$:Tm (10%) has increased 9.5- and 20-fold compared with that from $NaYF_4$:Yb/Tm (20%/1%) and $NaYF_4$:Yb/Tm (20%/10%) UCNPs (Figure 2c). Similarly, $NaYbF_4$:Er (50%) exhibits the strongest 660 nm intensity, 1.6- and 1.5-fold greater than that from $NaYF_4$:Yb/Er (20%/1%) and $NaYF_4$:Yb/Er (20%/50%) (Figure 2d). The results from Figure 2c,d indicate that the red emission intensity can only be enhanced by increasing both activator and sensitizer content. The following two factors contribute to the boost in red emission intensity: (1) The CR, albeit by an indirect route, induces the activators' excited

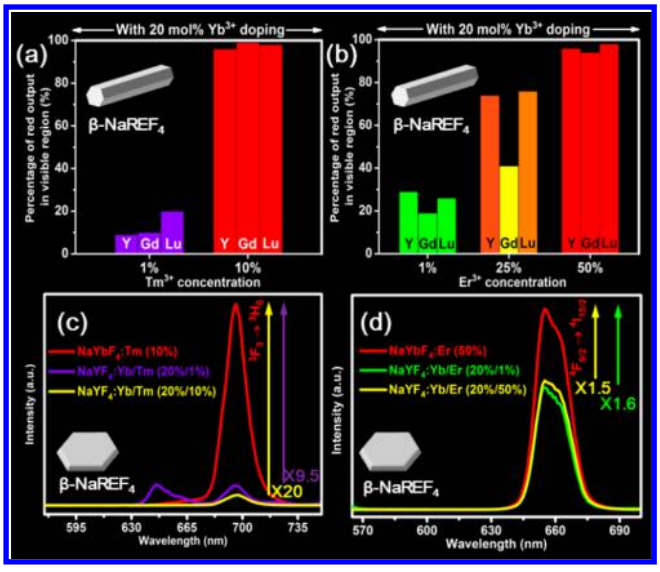

Figure 2. Percentage of red UC emission output in the visible region from (a) $NaREF_4$:Yb/Tm and (b) $NaREF_4$:Yb/Er microrods synthesized via a solvothermal method. RE represents Y^{3+}, Gd^{3+}, and Lu^{3+}, and the sensitizer Yb^{3+} was fixed at conventional 20 mol % doping for all the samples in (a) and (b). (c) 696 nm UC emission from $NaYbF_4$:Tm (10%), $NaYF_4$:Tm (20%/1%), and $NaYF_4$:Yb/Tm (20%/10%) UCNPs and (d) 660 nm UC emission from $NaYbF_4$:Er (50%), $NaYF_4$:Er (20%/1%), and $NaYF_4$:Yb/Er (20%/50%) UCNPs synthesized via a coprecipitation method. The spectra were recorded with 1 wt % UCNPs dispersed in hexane under 980 nm laser excitation at a power of 600 mW. Note: the insets of (a), (b), (c), and (d) show the diagrammatic representation of the as-synthesized microrods (a and b) and UCNPs (c and d), of which the same type of particles were compared.

electrons from the nonred to the red radiative excited states (CR mechanism discussed below). (2) The increase in

dx.doi.org/10.1021/cm5022382 | Chem. Mater. 2014, 26, 5183−5186

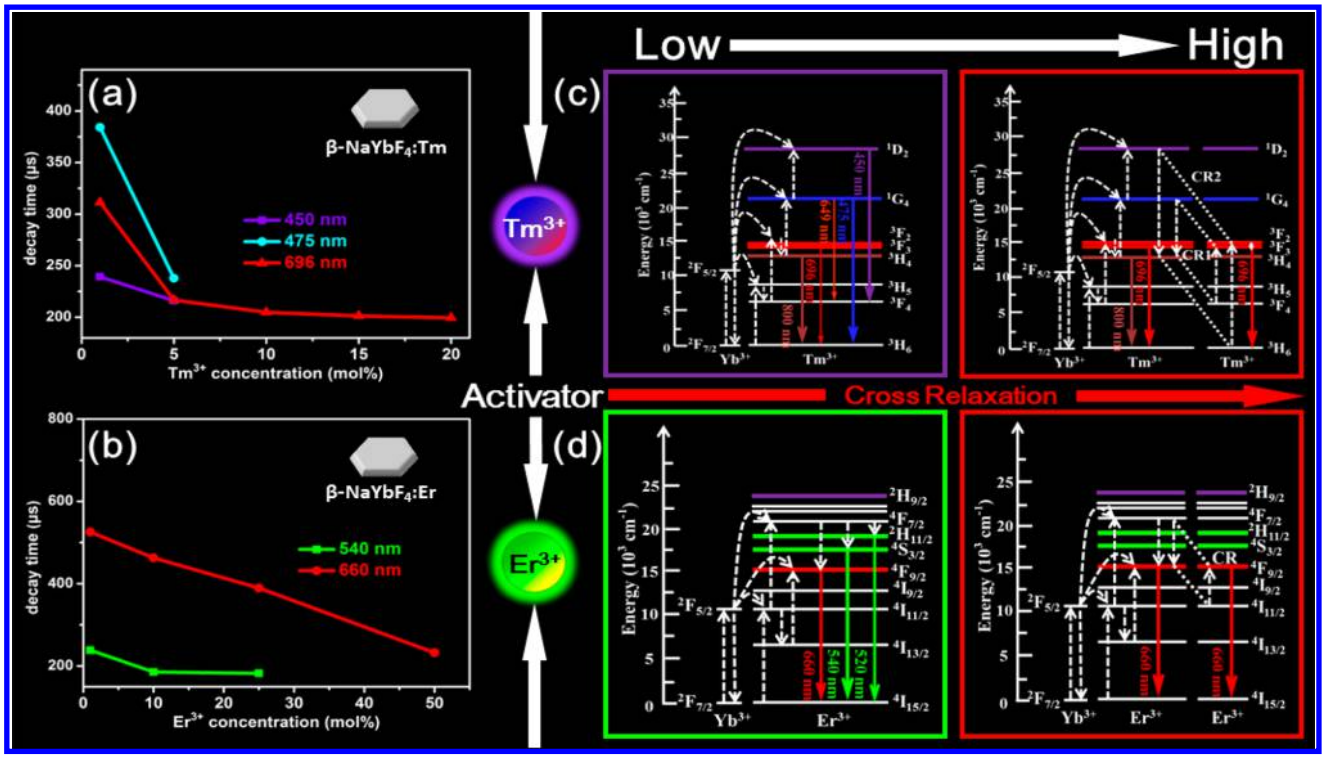

Figure 3. (a) Fluorescence decay times of the UC emissions at 450, 475, and 696 nm as a function of Tm^{3+} concentration in $NaYbF_4$:Tm UCNPs. (b) Fluorescence decay times of the UC emissions at 540 and 660 nm as a function of Er^{3+} concentration in $NaYbF_4$:Er UCNPs. Proposed UC mechanisms of (c) Tm^{3+} and (d) Er^{3+} at low and high concentration doping levels, respectively. Note that the UC mechanism involves CR effect at high activator (Tm^{3+} or Er^{3+}) doping level.

sensitizer content ensures enhanced absorption of excitation photons and thus increasing the ET from sensitizer to activator.

To further understand the underlying UC mechanism of the current CR effect induced pure red emission output, we undertook power dependence of the UC fluorescence intensity and fluorescence lifetime studies. The 450, 475, 649, and 696 nm emissions from Tm^{3+} doped UCNPs are determined to be four-, three-, three- and two-photon UC processes (Supporting Information Figure S3); both 540 and 660 nm emissions from Er^{3+} doped UCNPs are two-photon UC processes (Supporting Information Figure S4). By analyzing the data from Supporting Information Figures S5 and S6, their corresponding decay times τ_{decay} are listed in Supporting Information Tables S4 and S5. Subsequently, we plotted the fluorescence τ_{decay} of selected emissions as a function of activator concentration (Figure 3a,b). It is evident that the τ_{decay} of the selected emissions manifest a diminishing trend with the increase of activator content. In Figure 3a, the τ_{decay} of 450 and 475 nm emissions arisen from the $^1D_2 \rightarrow {}^3F_4$ and $^1G_4 \rightarrow {}^3H_6$ transitions are absent above 5 mol % Tm^{3+} doping, and we ascribe this to the increased CR effect among the Tm^{3+} activator, leading to a sharp decline of 450 and 475 nm emissions τ_{decay}.[12] Therefore, their fluorescence decay times are much shorter than that of 696 nm (approximately 200 μs) originated from the $^3F_3 \rightarrow {}^3H_6$ transition when Tm^{3+} doping is above 5%,[12a] supporting the quenching of 450 and 475 nm emissions. In the case of Er^{3+} doped UCNPs, the fluorescence lifetime of the 660 nm emission due to the $^4F_{9/2} \rightarrow {}^4I_{15/2}$ transition is much longer than the 540 nm emission from the $^4S_{3/2} \rightarrow {}^4I_{15/2}$ transition at low or high Er^{3+} doping (Figure 3b). The CR effect among Er^{3+} results in a drastic τ_{decay} decrease of 540 nm emission when the concentration of Er^{3+} is above 25%, resulting in the disappearance of 540 nm and a relatively long-lived 660 nm emission.

An energy transfer mechanism is proposed for the current CR-induced UC pure red emission. As depicted in Figure 3c, when Tm^{3+} content is very low, CR has very little influence on the UC process, and the $^1G_4$ and $^1D_2$ energy levels can be efficiently populated. However, when Tm^{3+} content is high, the CR1: [$^1G_4 \rightarrow {}^3H_4$ (8680 cm^{-1}): $^3F_4 \rightarrow {}^3F_3$ (−8380 cm^{-1})] and CR2: [$^1D_2 \rightarrow {}^3H_4$ (15240 cm^{-1}): $^3H_6 \rightarrow {}^3F_2$ (−14800 cm^{-1})] processes may readily take place due to a small energy mismatch (about 300 cm^{-1} for CR1 and 440 cm^{-1} for CR2 as determined from Supporting Information Table S6). CR1 dramatically depopulates the $^1G_4$ energy level and thus is responsible for the quenching of 475 nm emission, while CR2 provides a reasonable explanation for the quenching of 450 nm emission resulting from the drastic depopulation of the $^1D_2$ energy level at high Tm^{3+} doping. This is very different from the widely accepted CR [$^3F_3 \rightarrow {}^3H_6$: $^3F_3 \rightarrow {}^1D_2$],[5b,13] which explains the population in the $^1D_2$ energy level. Thus, CR1 and CR2 collectively improve the population of the $^3F_{2,3}$ energy levels, resulting in the rise of 696 nm red emission, despite being a strong function of the excitation photon flux due to the involvement of three- and four-photon processes. Similarly, the system with high Er^{3+} concentration (a two-photon process), CR: [$^4F_{7/2} \rightarrow {}^4F_{9/2}$ (5190 cm^{-1}): $^4I_{11/2} \rightarrow {}^4F_{9/2}$ (−5030 cm^{-1})], may readily occur given the small energy mismatch (about 160 cm^{-1} as determined from Supporting Information Table S6) when Er^{3+} content is high (Figure 3d).[14] The above CR effect can be employed as a tool to indirectly induce the excited electrons from the nonred to red radiative excited states, of which the Er^{3+} system may be more suitable for deep tissue imaging as it is not severely limited by photon flux. Note that

dx.doi.org/10.1021/cm5022382 | Chem. Mater. 2014, 26, 5183−5186

the CR induced red emission intensification is not applicable for Ho^{3+} doped UCNPs (Supporting Information Figure S7).

The original oleic acid coated $NaYbF_4$:Tm (10%) UCNPs were modified with citric acid[2b,15] and demonstrated in dual-modal fluorescent/CT imaging. The cytotoxicity assessment was performed based on the requirement of our in vitro bioimaging experiments (10 μg/mL) as well as existing works from other groups,[16] and the results manifested minimal cytotoxicity (Supporting Information Figure S8). Intense visible UC red signal could be detected from the SiHa cells cultured with the modified $NaYbF_4$:Tm (10%) UCNPs (Supporting Information Figure S9a). Supporting Information Figure S9b presents the bright field image of SiHa cells, and the nuclei (blue) of these cells were stained with DAPI (Supporting Information Figure S9c). The merged image (Supporting Information Figure S9d) indicates the successful internalization of the citric acid modified $NaYF_4$:Yb/Tm (10%) UCNPs. The phantom CT images show clear evidence that the Yb^{3+}-rich $NaYbF_4$:Tm (10%) UCNPs offer a better CT contrast compared to clinically used Iohexol (Supporting Information Figure S10a) and Y^{3+}-rich $NaYF_4$:Yb/Tm (20%/1%) UCNPs. From the resulting Hounsfield units (HU) (Supporting Information Figure S10b), the contrast efficiency of $NaYF_4$:Yb/Tm (10%) UCNPs was approximately two times of that of Iohexol and four times higher than that of $NaYF_4$:Yb/Tm (20%/1%) UCNPs. Hence, the results confirm that $NaYbF_4$:Tm (10%) UCNPs are a promising contrast agent for CT imaging.

In conclusion, the current discovery of CR effect induced intense pure red UC phenomenon provides us with new insights into activator- and sensitizer-rich UC mechanism in UCNPs, while allowing us to precisely manipulate the UC color output through CR effect by tuning the activator content. By harnessing the attributes of sensitizer-rich $NaYbF_4$ host for yielding pure red UC emission at high activator content and Yb^{3+} ions' high X-ray absorption coefficient, its potential application as a dual-modal contrast agent in CT/fluorescence deep tissue imaging has been demonstrated.

■ ASSOCIATED CONTENT

Ⓢ Supporting Information

Additional experimental details. This material is available free of charge via the Internet at http://pubs.acs.org.

■ AUTHOR INFORMATION

Corresponding Author

*E-mail: tytan@ntu.edu.sg.

Notes

The authors declare no competing financial interest.

■ ACKNOWLEDGMENTS

We thank Dr. Liu Yang for assistance with cell viability studies. This work was supported by Singapore Ministry of Education AcRF Tier 2 ARC16/11. Prof. Sun Handong acknowledges the financial supports from the Singapore National Research Foundation through the Competitive Research Programme (CRP) under Project Nos. NRF-CRP5-2009-04 and NRF-CRP6-2010-02.

■ REFERENCES

(1) (a) Tu, D.; Liu, L.; Ju, Q.; Liu, Y.; Zhu, H.; Li, R.; Chen, X. *Angew. Chem., Int. Ed.* **2011**, *50*, 6306. (b) Das, G. K.; Tan, T. T. Y. *J. Phys. Chem. C* **2008**, *112*, 11211. (c) Hu, W.; Lu, X.; Jiang, R.; Fan, Q.; Zhao, H.; Deng, W.; Zhang, L.; Huang, L.; Huang, W. *Chem. Commun.* **2013**, *49*, 9012. (d) Wei, W.; He, T.; Teng, X.; Wu, S.; Ma, L.; Zhang, H.; Ma, J.; Yang, Y.; Chen, H.; Han, Y.; Sun, H.; Huang, L. *Small* **2012**, *8*, 2271. (e) Idris, N. M.; Gnanasammandhan, M. K.; Zhang, J.; Ho, P. C.; Mahendran, R.; Zhang, Y. *Nat. Med.* **2012**, *18*, 1580.

(2) (a) Wang, Y.-F.; Liu, G.-Y.; Sun, L.-D.; Xiao, J.-W.; Zhou, J.-C.; Yan, C.-H. *ACS Nano* **2013**, *7*, 7200. (b) Sun, Y.; Zhu, X.; Peng, J.; Li, F. *ACS Nano* **2013**, *7*, 11290. (c) Zhu, X.; Zhou, J.; Chen, M.; Shi, M.; Feng, W.; Li, F. *Biomaterials* **2012**, *33*, 4618. (d) Zhang, Y.; Wei, W.; Das, G. K.; Tan, T. T. Y. *J. Photochem. Photobiol., C* **2014**, *20*, 71.

(3) (a) Wang, J.; Wang, F.; Wang, C.; Liu, Z.; Liu, X. *Angew. Chem., Int. Ed.* **2011**, *50*, 10369. (b) Zhang, Y.; Lin, J. D.; Vijayaragavan, V.; Bhakoo, K. K.; Tan, T. T. Y. *Chem. Commun.* **2012**, *48*, 10322.

(4) Yi, G. S.; Chow, G. M. *Adv. Funct. Mater.* **2006**, *16*, 2324.

(5) (a) Wang, F.; Deng, R.; Wang, J.; Wang, Q.; Han, Y.; Zhu, H.; Chen, X.; Liu, X. *Nat. Mater.* **2011**, *10*, 968. (b) Wang, F.; Liu, X. *Acc. Chem. Res.* **2014**, *47*, 1378. (c) Chen, G.; Qiu, H.; Prasad, P. N.; Chen, X. *Chem. Rev.* **2014**, *114*, 5161.

(6) (a) Wang, F.; Liu, X. *Chem. Soc. Rev.* **2009**, *38*, 976. (b) Misiak, M.; Prorok, K.; Cichy, B.; Bednarkiewicz, A.; Stręk, W. *Opt. Mater.* **2013**, *35*, 1124.

(7) Xing, H.; Zheng, X.; Ren, Q.; Bu, W.; Ge, W.; Xiao, Q.; Zhang, S.; Wei, C.; Qu, H.; Wang, Z.; Hua, Y.; Zhou, L.; Peng, W.; Zhao, K.; Shi, J. *Sci. Rep.* **2013**, *3*, 1751.

(8) (a) Teng, X.; Zhu, Y.; Wei, W.; Wang, S.; Huang, J.; Naccache, R.; Hu, W.; Tok, A. I. Y.; Han, Y.; Zhang, Q.; Fan, Q.; Huang, W.; Capobianco, J. A.; Huang, L. *J. Am. Chem. Soc.* **2012**, *134*, 8340. (b) Wang, F.; Han, Y.; Lim, C. S.; Lu, Y.; Wang, J.; Xu, J.; Chen, H.; Zhang, C.; Hong, M.; Liu, X. *Nature* **2010**, *463*, 1061.

(9) Prorok, K.; Bednarkiewicz, A.; Cichy, B.; Gnach, A.; Misiak, M.; Sobczyk, M.; Strek, W. *Nanoscale* **2014**, *6*, 1855.

(10) (a) Su, J.; Song, F.; Tan, H.; Han, L.; Zhou, F.; Tian, J.; Zhang, G.; Cheng, Z.; Chen, H. *J. Phys. D: Appl. Phys.* **2006**, *39*, 2094. (b) Wang, H.; Yi, Z.; Rao, L.; Liu, H.; Zeng, S. *J. Mater. Chem. C* **2013**, *1*, 5520.

(11) Chen, G.; Qiu, H.; Fan, R.; Hao, S.; Tan, S.; Yang, C.; Han, G. *J. Mater. Chem.* **2012**, *22*, 20190.

(12) (a) Lu, Y.; Zhao, J.; Zhang, R.; Liu, Y.; Liu, D.; Goldys, E. M.; Yang, X.; Xi, P.; Sunna, A.; Lu, J.; Shi, Y.; Leif, R. C.; Huo, Y.; Shen, J.; Piper, J. A.; Robinson, J. P.; Jin, D. *Nat. Photonics* **2014**, *8*, 32. (b) Zhang, H.; Li, Y.; Lin, Y.; Huang, Y.; Duan, X. *Nanoscale* **2011**, *3*, 963. (c) Bai, X.; Li, D.; Liu, Q.; Dong, B.; Xu, S.; Song, H. *J. Mater. Chem.* **2012**, *22*, 24698.

(13) Zheng, K.; Liu, Z.; Lv, C.; Qin, W. *J. Mater. Chem. C* **2013**, *1*, 5502.

(14) Vetrone, F.; Boyer, J.-C.; Capobianco, J. A.; Speghini, A.; Bettinelli, M. *J. Appl. Phys.* **2004**, *96*, 661.

(15) Sun, Y.; Peng, J.; Feng, W.; Li, F. *Theranostics* **2013**, *3*, 346.

(16) (a) Wang, Z.-L.; Hao, J.; Chan, H. L. W.; Law, G.-L.; Wong, W.-T.; Wong, K.-L.; Murphy, M. B.; Su, T.; Zhang, Z. H.; Zeng, S. Q. *Nanoscale* **2011**, *3*, 2175. (b) Zhou, J.-C.; Yang, Z.-L.; Dong, W.; Tang, R.-J.; Sun, L.-D.; Yan, C.-H. *Biomaterials* **2011**, *32*, 9059.